Elastocaloric Effect in Vulcanized Natural Rubber and Natural/Wastes Rubber Blends

Nicolas Candau [1,*], Eduard Vives [2], Ana Inés Fernández [3], Maria Lluïsa Maspoch [1]

[1] Centre Català del Plàstic (CCP) - Universitat Politècnica de Catalunya Barcelona Tech (EEBE-UPC), Av. D'Eduard Maristany, 16, 08019, Spain

[2] Departament de Física de la Matèria Condensada, Facultat de Física, Universitat de Barcelona, Martí i Franquès 1-11, 08028 Barcelona, Spain

[3] Department of Materials Science and Physical Chemistry, Universitat de Barcelona, Martí i Franquès 1-11, 08028 Barcelona, Spain

[*]Corresponding author:

nico.candau@gmail.com

Abstract

Vulcanized natural/wastes rubber blends were prepared and their elastocaloric properties were analysed. A thermodynamic frame was used to discriminate the contributions of thermoelastic effects and strain induced crystallization/melting. The substitution of 20 wt.% of the natural rubber matrix by waste rubber particles resulted in a maintain and even a slight improvement of heat exchanges (+10%), that we ascribed to a *(i)* high thermoelastic effect and a *(ii)* a high ability of the natural rubber matrix to crystallize due to a nucleation ability of the waste particles, both resulting from a strain amplification in the rubber phase due to undeformable carbon black aggregates in the waste particles. The materials coefficient of performance, COP_{mat}, was estimated equal to 4.4 for the neat natural rubber and 3.8 for the blend containing 20 wt.% of wastes due to larger mechanical energy originated from reinforcing effect of waste particles. Nonetheless, the elastocaloric (eC) abilities of these materials, especially their wide temperature spans (similar to those in films or polycrystals using rare earth elements) make these natural/waste rubber blends good candidates for application such as heating/cooling machines. Moreover, the partial replacement of natural rubber, a bio-source material showing risks of shortage, by industrial wastes rubber, place these blends as promising eco-friendly materials with high added value.

1. Introduction

Sustainable energy technology and materials recycling are two fundamental topics that aim to contributing to reduce the environmental impact of materials and energy production. The development of sustainable energy respond to an increasing demand of regulating the temperature on the surface of our planet without increasing greenhouse emissions [1]. Caloric materials possess promising properties that can contribute to achieve this aim. They are solids that can exchange heat from the environment that include cooling and refrigeration applications. Nonetheless,

conventional caloric materials use rare-earth elements, are not only expensive but also prone to supply shortages. Refrigeration and cooling devices use a variety of rare earths with magnetic properties such as Gadolinium (Gd) or Neodymium (Nd) [2] or ferroelectric properties such as Neodymium (Nd) or Praseodymium (Pr) [3]. Hence, innovative solutions need to be investigated in order to overcome this issue that permit their efficient commercial applications while targeting economic and ecological concerns. Natural rubber (NR) is a promising candidate for green cooling applications [4].

Contrarily to most of the caloric materials, natural rubber is soft, cheap and biodegradable, simultaneously solving some of the major engineering and sustainability issues of artificial heating and/or cooling. To the best of our knowledge, the first qualitative observation of the elastocaloric (eC) effect in natural rubber has been reported by Gough in 1805 [5]. Gough described a “sensation of warmth” on rubber surface after fast stretching. Decades later, Joule [6] quantitatively reported a rise in heat by applying a tensile force. In 1942, Dart, Anthony and Guth reported further temperature measurements and suggested this heating to be ascribed to the strain induced crystallization (SIC) transition as shown by X-rays [7]. Such strain induced crystallization in rubber was predicted by Flory in 1947 [8]. The rubber chains alignment upon uniaxial loading causes a significant decrease of their conformational entropy. Then, less conformational entropy is needed to transform amorphous rubber chains into a crystalline state, and crystallization can occur without environmental temperature changes if a certain deformation is applied (typically 300% of the initial length of the rubber). Strain induced crystallization can be found in natural but also synthetic elastomers such as isoprene rubber (IR) [9], chloroprene rubber (CR) [10] or thermoplastic polyurethanes (TPU) [11,12]. Nonetheless, SIC in NR is known to be more effective as compared to other synthetic elastomers [13] that is commonly accepted to be partly due to the

high proportion of NR chains with cis 1,4 configuration (>98%) that facilitates their alignment upon deformation. The concept of entropic elasticity in rubber has been fully modelled [14] and currently developed models are physically based [15,16], within the light of microstructural properties accessible by X-ray synchrotron sources [17,18].

Nowadays, the eC effect in natural rubber is still a subject of active investigation [19,20,21,22]. Most of the experimental studies were aimed to optimize the eC effect: stretching level [19], strain rate and environmental temperature [22], etc. One practical advantage of eC properties in natural rubber is the possibility to modulate the strain induced crystallization kinetics with strain. At a deformation of 600%, its lowest crystallization time was found around few decades of milliseconds [24]. As a consequence, rubber can be heated rapidly up to a decade of degrees after the completion of its crystallization process. Another remarkable advantage of natural rubber is the weak mechanical energy required to activate its eC effect. It has a lower stress level as compared to the current standard vapor-compressors (two order of magnitude lower than in shape memory alloys), which proves its technical feasibility and facilitates technology transformation. Hence, the development of sustainable energies, such as heat pump or cooling machines based on eC effect of natural rubber has received a considerable interest from the academic community.

However, some works remain to do to make rubber an efficient eco-friendly eC material: *(i)* the partial replacement of the natural rubber matrix by waste rubber particles and *(ii)* a physical description of the eC effect in these natural/wastes rubber blends to fine tune the cooling properties. While natural rubber is more abundant that rare earth metals, it is also prone to a risk of supply shortages. To overcome this issue, natural rubber can be partially replaced by wastes. Moreover, the recycling of industrial waste rubber has received considerable attention in response to the increasing demand for sustainable solutions for worldwide disposal problem of waste

plastic/rubber [25,26]. The introduction of waste rubber into bio-based thermoplastics as a high-added value additive is an interesting alternative for rubber recycling, while at the same time providing toughened thermoplastics elastomers [27,28]. Nonetheless, it is a challenge to reintroduce waste rubber into the production cycle in the rubber industry as – in comparison to the fresh rubber – the added value is limited, especially for waste contents above 50 wt.%. Nonetheless, it has been shown that the incorporation of crystallizable wastes, such as waste Chloroprene rubber (CR) [29], waste Latex [30], or Ground Tire Rubber (GTR) [31] into NR enhances mechanical reinforcement of the resulting composites, that were attributed to their improved ability to crystallize under strain, as shown by direct in-situ X-rays observations in the case of NR/GTR blends [31]. In spite of these evidences of crystallization, and hence potential caloric properties in these above-mentioned natural/wastes rubber blends, their development as candidates for heating/cooling systems has received far less attention. To the best of our knowledge, only one published study focused on the characterization of barocaloric effects (observation of an adiabatic temperature change by applying an isostatic pressure) in natural/wastes rubber blends [32]. However, no insights were provided on the physical origins of the barocaloric effect in such materials, that is however of prime importance to fine-tune the materials composition to the optimization of heating/cooling properties.

This study is dedicated to the description of elastocaloric effect in natural/wastes rubber blends from both fundamental and applicative points of view. To this aim, we prepared a series of natural/wastes rubber blends with wastes content up to 33 wt.% and characterized them by infrared thermography. For the physical understanding of their eC properties, we used a thermodynamic frame able to predict both the heat variations and the mechanical behaviour arising from thermoelastic effects. Deviations from this model traduce the occurrence of strain induced

crystallization. Results revealed that highest heat exchanges were observed for natural/wastes rubber blend using 20 wt.% of wastes that were ascribed to *(i)* an improved thermoelastic effect and *(ii)* an improved ability of the natural rubber matrix to crystallize, both resulting from a strain amplification in the rubber phase in presence of undeformable carbon black aggregates in the waste particles. This resulted in a materials coefficient of performance, COP_{mat}, of 3.8 in the natural/wastes rubber blends containing 20 wt.% of wastes that was found close to the one in neat NR (COP_{mat}= 4.4). These natural/wastes rubber blends show a potential for eco-friendly heating/cooling applications, especially due to their great temperature spans, in the range of the ones found in films or polycrystals using rate earth elements.

2. Materials and experiments

2.1. Materials and processing

The natural rubber (NR) of this study is an SMR (Standard Malaysian Rubber) CV60 (Mooney Viscosity ML 1+4, 100 °C: 55-60), supplied by the company Akrochem (USA), with 0,15% of hydroxylamine added to the latex stage to prevent the raw rubber stiffening while storing. Ground tire rubber (GTR) was supplied by the company J. Allcock & Sons Ltd (United Kingdom) using the transformation of tire buffing into finer rubber crumbs via a controlled cryo-grinding. GTR is composed of 55 wt.% of rubber (85 wt.% of natural rubber, NR, and 15 wt.% of Styrene Butadiene Rubber, SBR) and 45 wt.% of carbon black, CB. The GTR crumbs are free of contaminants such as textile, metal and road dirt. The GTR particles were subsequently sieved using a vibratory sieve shaker (Analysette 3, Germany) with a mesh 120's (size <125 μm). Before processing, the GTR particles were dried overnight in a vacuum oven (Vaciotem-TV, J.P. SELECTA®, Spain) to prevent humidity absorption, over silica gel at 70 °C to remove any moisture. The natural rubber was masticated inside the chamber of an internal mixer (Brabender Plastic-Corder W50EHT,

Brabender GmbH & Co., Germany) at a temperature of 80 °C, for 5 minutes and a rotation speed of 40 rpm. After 5 minutes of mastication, the GTR was added. After 5 more minutes the vulcanizing agent dicumyl peroxide (DCP) was added (1.5 wt.% of the NR) and mixed for 5 minutes. The masterbatch containing NR, GTR and DCP was vulcanized according to the estimated optimal time at 170 °C [33] under 4 MPa. In order to perform the tensile test (section 2.2), dogbone shaped specimens with a 1 mm thickness, 4 mm width and 15 mm length were extracted from hot moulded sheets by die-cutting with a specimen preparation punching machine (CEAST). **Table 1** gives the main composition and properties of the prepared materials. The CB content is calculated accounting for the total rubber content (NR matrix and NR and SBR contained into the GTR particles). The volume percent of carbon black is calculated using a density of 1.9 $g.mol^{-1}$ for the CB particles and of 0.92 $g.mol^{-1}$ for the rubber phase. The density, ρ, is calculated following a simple rule of mixture and from the knowledge of the density and weight fraction of the rubber phase and carbon black particles. The specific heat capacity, Cp, and the thermal conductivity, κ, are calculated from the data available in the literature for both vulcanized NR and NR/GTR blends. The rubber volume fraction, φ_r, corresponds to the total rubber fraction available in the blends (both the NR matrix and the NR and SBR contained into the GTR particles).

Table 1. Specimen nomenclature, composition and thermal properties at room temperature.

Sample code	NR	NR/GTR10	NR/GTR20	NR/GTR33
Waste particles, GTR (wt.%)	0.0	10.0	20.0	33
Carbon black, CB (wt.%)	0.0	4.5	9.0	14.9
Carbon black, CB (vol.%)	0.0	2.2	4.6	7.8
Carbon black, CB (phr)	0.0	4.8	10.0	18.1
Rubber fraction, φ_r (vol.%)	100	97.8	95.4	92.2
Density, ρ (g.cm^{-3})	0.92	0.94	0.96	0.99
Specific heat capacity, Cp (J.g^{-1}K^{-1}) [34]	1.88	1.85	1.82	1.78
ρCp (MJ.m^{-3}.K^{-1})	1.73	1.74	1.75	1.77
Thermal conduct. κ (W.K^{-1}.m^{-1}) [35]	0.15	0.17	0.18	0.19

2.2. High strain rate tensile tests probed by Infra-red thermography measurements

Room temperature uniaxial tensile tests were performed on a universal testing machine ZwickRoell (Z005) equipped with a 5 kN force sensor. The crosshead speed during the loading and unloading phases was chosen equal to of 3000 mm/min corresponding to a nominal strain rate of 2×10^2 min^{-1} according to the specimen dimensions (15 mm length). In a first type of tensile tests, the rubber specimens were stretched during single uniaxial stretching up to failure. In a second type of tensile tests, the rubber specimens were rapidly stretching with the nominal strain rate of 2×10^2 min^{-1} up to a deformation of 500% followed by a relaxation step in the deformed state for one minute. After the relaxation step, the specimens were unloaded with the same nominal strain rate of 2×10^2 min^{-1} down to the relaxed state (zero force) followed by another relaxation for one more minute. The correct specimen deformation was estimated by measuring the local deformation between two white lines drawn in the central part of the specimen, separated by an

initial distance of 10 mm and orthogonal to the specimen tensile axis. The local strain rate accounting for this correction has been estimated and found to slightly decrease with applied strain, but not in a significant manner (it is equal to 2×10^2 min^{-1} near undeformed state and 1.6×10^2 min^{-1} for highest applied deformation of 500%).

The temperature field on the front face of the samples was recorded using an Infra-red (IR) camera (InfraTech ImageIR® 8800) equipped with a Mercury-Cadmium-Telluride (MCT) detector with a temperature resolution at 30 °C higher than 0.035 K. The distance between the IR camera and the specimen was chosen sufficiently large to ensure that the sample surfaces can be observed from the undeformed state to the deformed state, but sufficiently low to record images with sufficiently fine pixel size (200 μm). The size of the observation zone (see **Figure 1**) is 160*500 $pixels^2$ (32*100 mm^2). Image data was synchronized with analogical data of the tensile test machine, namely time, force and displacement between the grips. The acquisition frequency of the IR images was chosen equal to 100 Hz in order to capture fast temperature changes that may occur withing the different phases of the tests. These frequencies are high enough to ensure a sufficiently low strain increment between two images during the loading and/or unloading (maximum of 8% of deformation) or sufficiently fast acquisition time during relaxation steps (10 ms). The IRBIS 3.1 professional software (InfraTech ImageIR® 8800) was used to extract punctual temperature values along the specimen longitudinal axis. The central part of the specimen where the temperature data was extracted shows a rather homogeneous temperature field at the mm scale (**Figure 1)**.

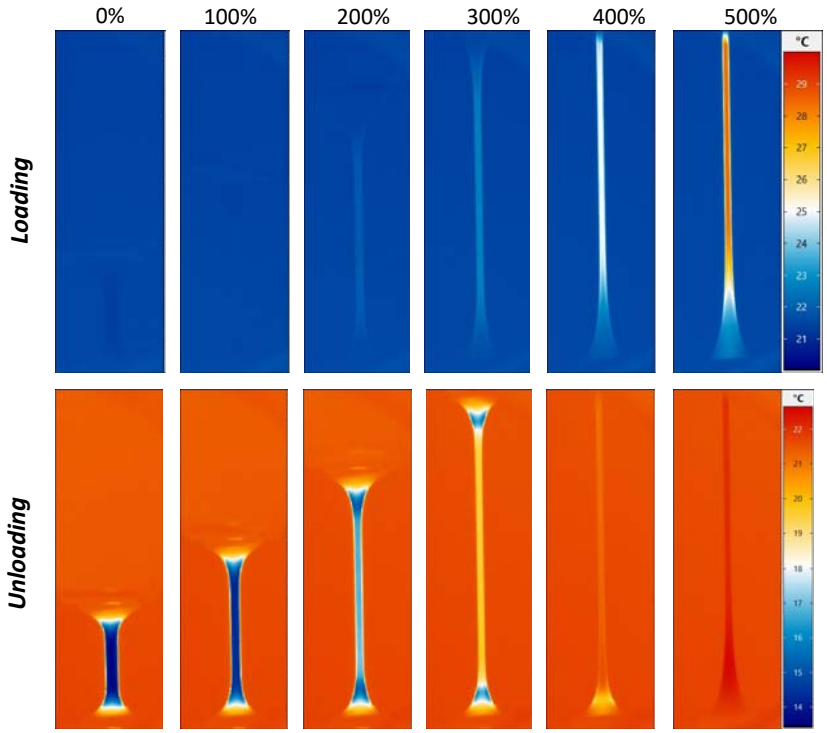

Figure 1. Temperature field measured on the specimen surface during loading (top figures) and unloading (bottom figures for various deformations: 0%, 100%, 200%, 300%, 400% and 500% from left to right. The specimen chosen for illustrating the temperature field here is the vulcanized natural rubber (NR).

3. Results and discussion

3.1. Single loading in NR and NR/GTR blends

Vulcanized natural rubber (NR) and natural rubber / ground tire rubber (NR/GTR) blends stretched at high strain rate (2×10^2. min^{-1}) up to failure show a hyper-elastic behaviour with a notable large strain reinforcement (**Figure 2**). To elucidate the origin of such reinforcement, stress strain curves are fitted with the gaussian approximation, where the decreased in chains entropy upon stretching results in an elastic force written as follows [36]:

$$\sigma_{g,1} = \nu RT \frac{\langle r^2 \rangle}{\langle r^2 \rangle_0} \left(\lambda - \frac{1}{\lambda^2} \right) \quad (1)$$

ν is the network chains density (in mol.cm^{-3}), R=8.314 J.K^{-1}.mol^{-1}, is the gas constant, T is the temperature (in K), $\lambda_c = 1 + \varepsilon$ is the stretching ratio, ε is the strain, r is the end-to-end distance of a chain from one cross-link to another in the crosslinking network, $\langle r^2 \rangle_0$ and $\langle r^2 \rangle$ represent the dimensions of the free chains in the unstretched and stretched states respectively.

One may note however that the gaussian approximation is not suitable for high deformation values. The observed mechanical reinforcement above ε=300% may originate from different phenomena, namely limited linear extension of chains, distribution of molecular mass between crosslinks, intermolecular (moieties) interactions and strain induced crystallization (SIC). The Edwards-Vilgis approach of finite network extensibility to the classical inverse Langevin function is commonly accepted for high deformation values [37]. Nonetheless, here as a first approach we consider the deviation of tensile curve from the gaussian approximation to be mostly representative of the occurrence of SIC. Indeed, tests performed at 80 °C, a temperature sufficiently high to avoid any SIC, can be well fitted by the gaussian approximation in the strain range studied, [31].

A simplified form of equation 1 [38] assumes $\langle r^2 \rangle$ to be identical to $\langle r^2 \rangle_0$, which means that the cross-links do not significantly change the chain dimensions from their unperturbed values, and hence the expression of the stress from gaussian approximation can be written:

$$\sigma_{g,2} = \nu RT \left(\lambda - \frac{1}{\lambda^2} \right) \quad (2)$$

With $\nu RT = E/3$, which provides the relation between the crosslink density of the rubber chains, ν, and the elastic modulus of the blend, E (in MPa). The elastic modulus is interpreted as the one of the rubber matrix, assuming the mechanical reinforcement due to the presence of fillers to be translated by the strain amplification factor. One may note that the gaussian distribution of the end-to-end distance r is generally not a good approximation for filled rubbers. Indeed, the

adsorption of polymer chains onto filler particles expectedly changes the mean value and the distribution of end-to-end vectors of the chains [39]. Nonetheless, a low filler content is expected to result in moderate modification of these values. In our materials, the quantity of carbon black is assumed sufficiently low (2.1, 4.3 and 7.5 vol.% for NR/GTR10, NR/GTR20 and NR/GTR33 respectively, see **Table 1**) so that the deviation from the gaussian approximation used for unfilled rubber is expected to not be meaningful.

As our tests are performed at high strain rate, temperature changes in the specimens are expected, hence the decreased entropy upon stretching results in an elastic force that depends not only on the temperature but also on the thermal dilatation of the materials. One may note that the adiabatic gaussian approximation is compulsory to detect phenomena such as the thermoelastic inversion effect that occurs at few precents of deformation (<10%) [36] but must also be maintained at larger strain especially in presence of wide internal temperature changes. The stress in the gaussian approximation and in adiabatic conditions is written [36]:

$$\sigma_{g,3} = \nu RT\left(\lambda - \frac{1+\alpha(T-T_0)}{\lambda^2}\right) \quad (3)$$

With T_0 is the temperature at the beginning of the test, α is the coefficient of thermal dilatation which is equal to 5. 10^{-4}.K^{-1} in the case of vulcanized natural rubber [36]. This coefficient has been found very nearly the same for the filled and unfilled natural rubbers at temperatures above the glass transition, T_g, [40] which is the frame of our experiments. Hence, in the following, we will assume the coefficient of thermal dilatation in the NR/GTR blends to be equal to the one of the neat natural rubber.

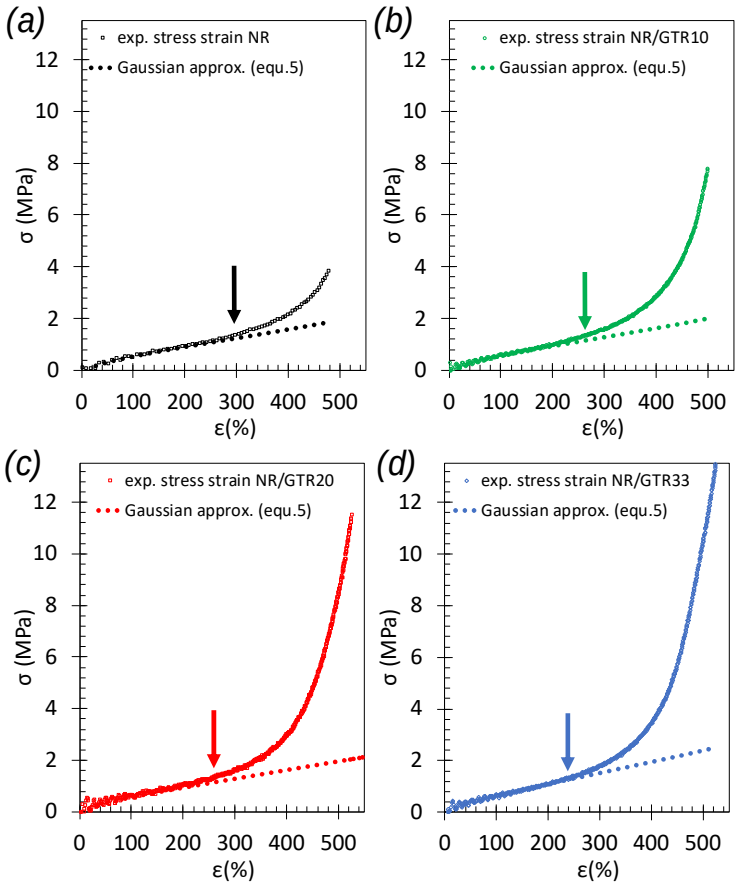

Figure 2. *(a, b, c, d)* stress-strain curves (solid lines) during uniaxial single loading performed at room temperature and at the nominal strain rate of 2×10^2 min^{-1} for the series of rubber: NR, NR/GTR10, NR/GTR20 and NR/GTR33. The dotted lines represent the fitting using the gaussian approximation (equation 3) and the arrows indicate the strain at which a deviation between experimental curves and the gaussian approximation is observed. From this fit, the network chains density that is the only output parameter in equation 3 is deduced and shown in **Table 1**.

From micro computed-tomography (µCT) observation [31], the highly dense GTR particles are indicative of a significative carbon black (CB) content. This is consistent with Thermogravimetric analysis (TGA) tests showing the GTR particles to contain ~45 wt.% of carbon black (CB) [28]. The CB particles not only increase the local strain in the NR matrix but also in the rubber phase (the latter also contains Styrene butadiene Rubber, SBR) of the GTR themselves. A strain

amplification factor, A, deduced from the Guth and Gold equation [41] is used to describe the local strain in the rubber phase account from the presence of carbon black particles:

$$A = \frac{\lambda_{local} - 1}{\lambda - 1} = 1 + 2.5\varphi_f + 14{\varphi_f}^2 \quad (4)$$

with λ_{local} the local strain in the whole rubber phase (NR matrix and NR/SBR phases in the GTR) and φ_f the volume fraction of the carbon black particles (**Table 1**). Such amplification factor is shown in **Figure 3** as a function of the carbon black content. In previous tensile tests carried out at slow strain rate (non-adiabatic conditions), we determined the strain at reinforcement onset of the same materials, that we measured experimentally from the deviation of the stress-strain curve from the room temperature gaussian approximation (equation 2), and deduced from equation 4 the amplification factor for each materials [31]. The experimental strain amplification deduced from that study (represented here by the data points in **Figure 3**) are found to follow the prediction from equation 4, and hence reinforce the correctness of such factor to apply to the measure of the local strain while describing large strain mechanisms.

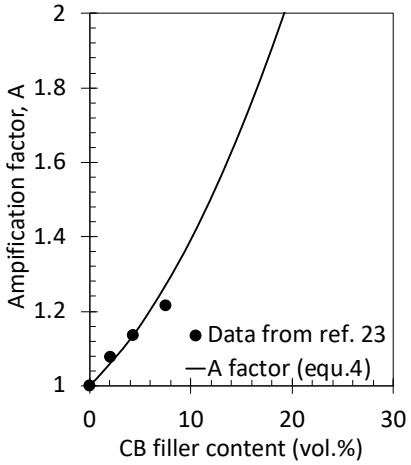

Figure 3. Theoretical amplification factor deduced from equation 4 (line). Experimental amplification factor extracted from a study performed in non-adiabatic conditions (slow strain rate) [31].

By combining equations 3 and 4, the gaussian approximation applied to our materials accounting for *(i)* the temperature changes on the specimen surface and *(ii)* the strain amplification due to the presence of CB particles, is written as follows:

$$\sigma_{g,4} = \nu RT\left(\lambda_{local} - \frac{1+\alpha(T-T_0)}{{\lambda_{local}}^2}\right) \quad (5)$$

This modified gaussian approximation is used to fit the experimental stress-strain curves (**Figure 2**). The network chains density, ν, is the only output parameter, and is found around 1.2×10^{-4} mol.cm^{-3} for all materials, suggesting the presence of wastes rubber particles to not modify the elastic properties of the rubber matrix. This may be ensured by the same weight fraction of peroxide as compared to natural rubber phase introduced into the blends. Up to a strain around 300% for the natural rubber and slightly less for the NR/GTR blends, equation 5 fits well the experimental data. ν being not dependent on the studied materials, the increased stress while increasing GTR content is found to be mostly due to the strain amplification effect. At higher strains, stress strain curves diverge from the gaussian approximation, more significantly in the NR/GTR blends. Such reinforcement results from the strain-induced crystallization in vulcanized NR [18] and has also been recently demonstrated in the case of NR/GTR blends [31].

Fast loading is associated with a self-heating on the rubber specimen surfaces (**Figure 4**) that may find several origins: thermoelastic effects and/or crystallization, as has been shown in the case of vulcanized natural rubber [22]. To confirm the respective contribution of thermoelastic effects and crystallization to heating, we estimate the temperature rise induced by the thermoelastic effect in the frame of the gaussian approximation:

$$\theta_{th-e} = \frac{T}{\rho C}\int_1^{\lambda}\left(\frac{\partial \sigma_{g,4}}{\partial T}\right)_{\lambda} d\lambda \quad (6)$$

$\sigma_{g,4}$ is given by equation 5. From the work of Guth [36], equation 6 results in an expression of the temperature change that we adapted for our study to account for the amplified local deformation in presence of carbon black particles:

$$\theta_{th-e} = \frac{\nu RT}{2\rho C}\left[{\lambda_{local}}^2 + \lambda_{local} - 2(1+\alpha T_0)\right]\left[\frac{\lambda_{local}-1}{\lambda_{local}}\right] \quad (7)$$

One may note that, in case the thermal dilatation is neglected (slow strain rate loading inducing non-adiabatic conditions or weak temperature changes) and in case the macroscopic deformation equals the local deformation (neat vulcanized rubber matrix), equation 7 reduces as follows:

$$\theta_{th-e} = \frac{\nu RT}{2\rho C}\left[\lambda^2 + \frac{2}{\lambda} - 3\right] \quad (8)$$

where $\nu RT/2\left[\lambda^2 + \frac{2}{\lambda} - 3\right]$ is the deformation energy assuming the simplest form of the gaussian approximation. We applied equation 7 to our experimental results (dotted lines in **Figure 4**) whose all parameters were fixed (values from the literature in **Table 1**, amplification factor from prior experiments in **Figure 2** and network chains density previously measured from tensile curves in **Figure 3**). The temperature increase estimated from equation 7 is found to follow the experimental data up to a strain corresponding to the strain upturn attesting for the occurrence of SIC. This suggests the description of thermoelastic effects assuming gaussian chains to nicely describe both mechanical and temperature experimental data in this strain range. Self-heating due to thermoelastic effects is found to increase while increasing GTR content that directly derives from the strain amplification effect as discussed earlier. The sudden increase of the temperature with strain at a critical strain around 300% for NR and slightly below for the NR/GTR blends (**Figure 4**) is concomitant with the deviation of the mechanical response from the Gaussian behaviour (**Figure 2)**, that we can ascribe to a transition from dominant thermoelastic (below the critical strain) to a dominant crystallization effect (above the critical strain).

One may note however that other dissipative mechanisms contributing to self-heating may occur. This is the case for carbon black or silica filled rubber that can undergo viscoelastic effect such as molecular sliding at filler/rubber interface [42], or damage arising from debonding/cavitation in the vicinity of the fillers [43,44,45]. Dissipative mechanisms at the interface between rubber and carbon black particles in the GTR particles are expected to be negligible in our materials due to the reasonable content of carbon black in our materials as compared to industrial filled elastomers [46]. However, distinct dissipative mechanisms such as molecular friction or chains breakage at NR/GTR interface can occur. Nonetheless, incremental loading on our materials have been shown to exhibit low permanent strain, with a maximum of 35% in NR/GTR33 [31], that is found three times lower than in conventional industrial filled deformed in close loading conditions [47]. This suggests that such dissipative mechanisms are not dominant in our materials and by inference they expect to not have strong impact on the heating response. However, the observation of temperature changes during mechanical cycles (section 3.2) and the calculation of associated heat sources (section 3.3) would permit to confirm or infirm such statement.

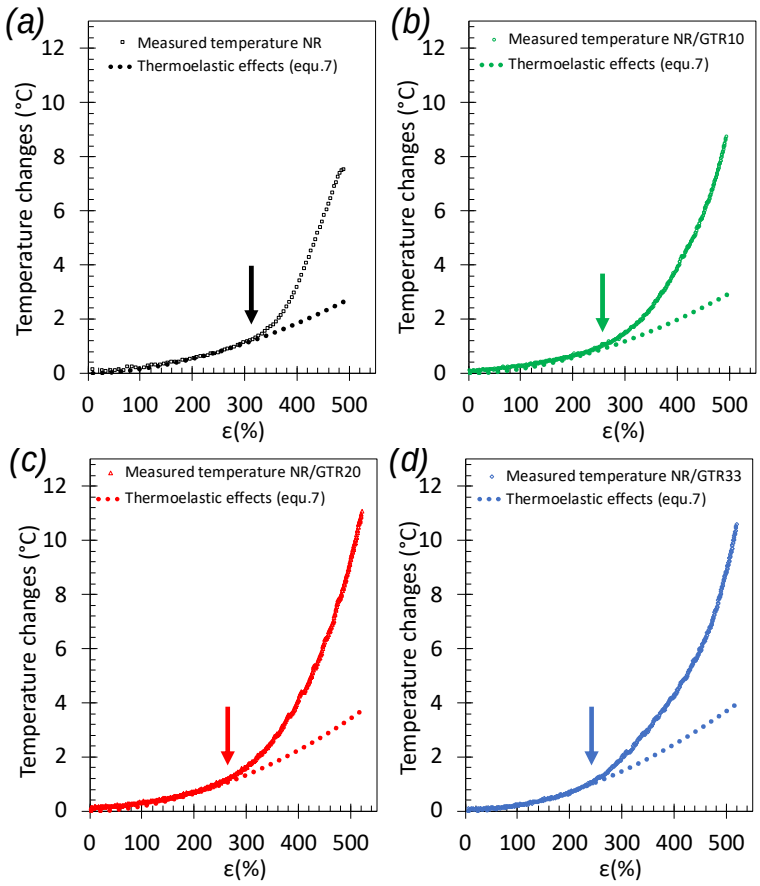

Figure 4. *(a, b, c, d)* temperature at the specimen surface measured on the center of the specimen for the same materials (solid lines) during uniaxial single loading performed at room temperature and at the nominal strain rate of 2×10^2 min^{-1} for the series of rubber: NR, NR/GTR10, NR/GTR20 and NR/GTR33. The dotted lines represent the fitting using the theoretical temperature rise due to thermoelastic effects within the gaussian approximation (equation 7) and the arrows indicate the strain at which a deviation between experimental data and the thermoelastic contribution. A deformation, ε, from 0 to 500% correspond to a stretching ratio, λ, from 1 to 6.

3.2. Cyclic loading in NR and NR/GTR blends

Dissipative thermoelastic and strain induced crystallization were shown to generate significant heating upon loading in both vulcanized NR and NR/GTR blends (section 3.1). Their cooling capacities are now studied by applying cyclic tests (**Figures 5-8**). To discriminate heating and cooling abilities, a one-minute relaxation step after loading was applied to permit a return to equilibrium room temperature. Same relaxation step was applied after unloading. The mechanical

hysteresis observed in both NR and NR/GTR blends (**Figure 5**) is mostly induced by a "superstraining" effect due to the difference in strain at crystallization and strain at melting, as described for natural rubber materials [48].

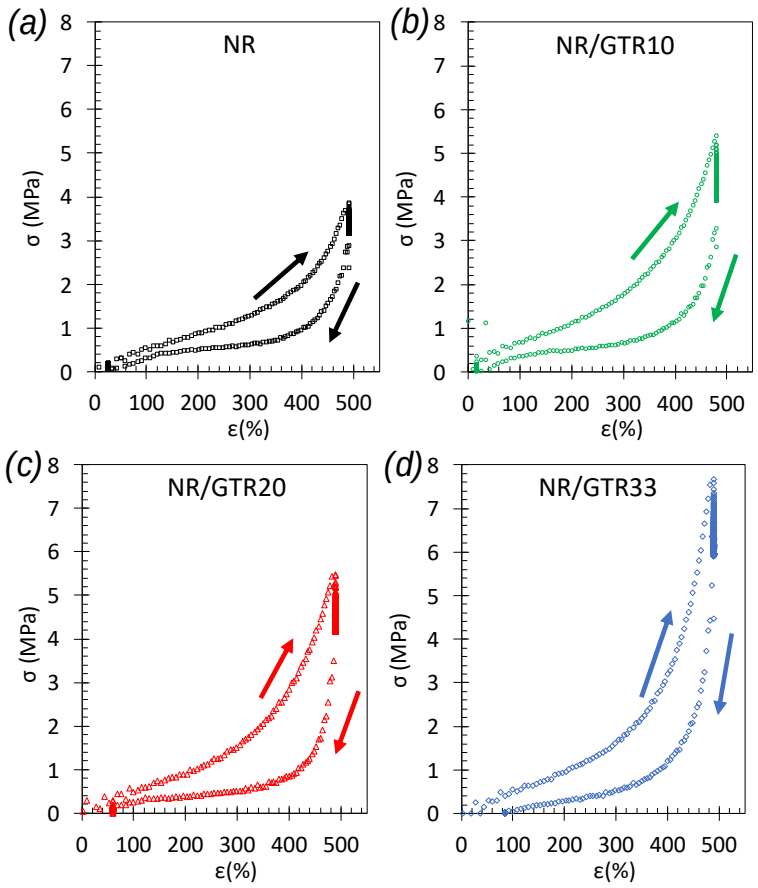

Figure 5. *(a, b, c, d)* stress-strain curves during cycles performed at room temperature for the series of rubber from left to right: NR, NR/GTR10, NR/GTR20 and NR/GTR33. A deformation, ε, from 0 to 500% correspond to a stretching ratio, λ, from 1 to 6.

The unloading is associated with a deep drop of the temperature (**Figure 6**), down to a minimum of 12.8 °C found for the natural rubber containing 20 wt.% of wastes (NR/GTR20) that was found slightly lower than the minimum temperature of 13.5 °C for the NR, hence showing the potential of natural/wastes rubber blends for cooling applications.

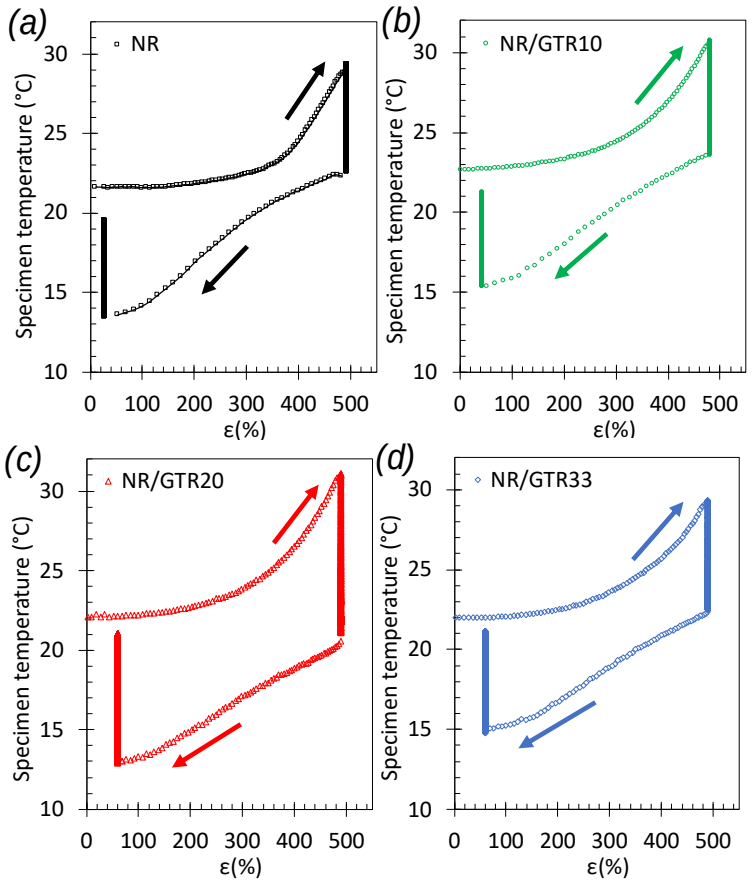

Figure 6. *(e, f, g, h)* corresponding temperature at the specimen surface measured on the center of the specimen for the same materials. The cyclic test consists of stretching with the nominal strain rate of 2×10^2 min^{-1} up to a deformation of 500% followed by a relaxation in the deformed state for one minute, and then unloading with the same nominal strain rate down to the relaxed state (null force) followed by another relaxation during one more minute. A deformation, ε, from 0 to 500% correspond to a stretching ratio, λ, from 1 to 6.

On a sufficiently large timescale (one minute), the relaxation steps are associated with a stabilization of the stress (**Figure 7a-d**) and a return to equilibrium temperature (**Figure 7e-h**) for the series of NR and NR/wastes rubber tested. Nonetheless, in spite of the significant heat generated during loading, that traduces a non-negligible amount of crystallization, the temperature indeed continues to increase during the relaxation step in the deformed state (**Figure 8**). Indeed, the fast strain rate applied may not allow the crystallization process to fully occur during the

loading [49,50] as strain induced crystallization kinetics may be limited by both crystal nucleation time and amorphous chains diffusion time [51,52].

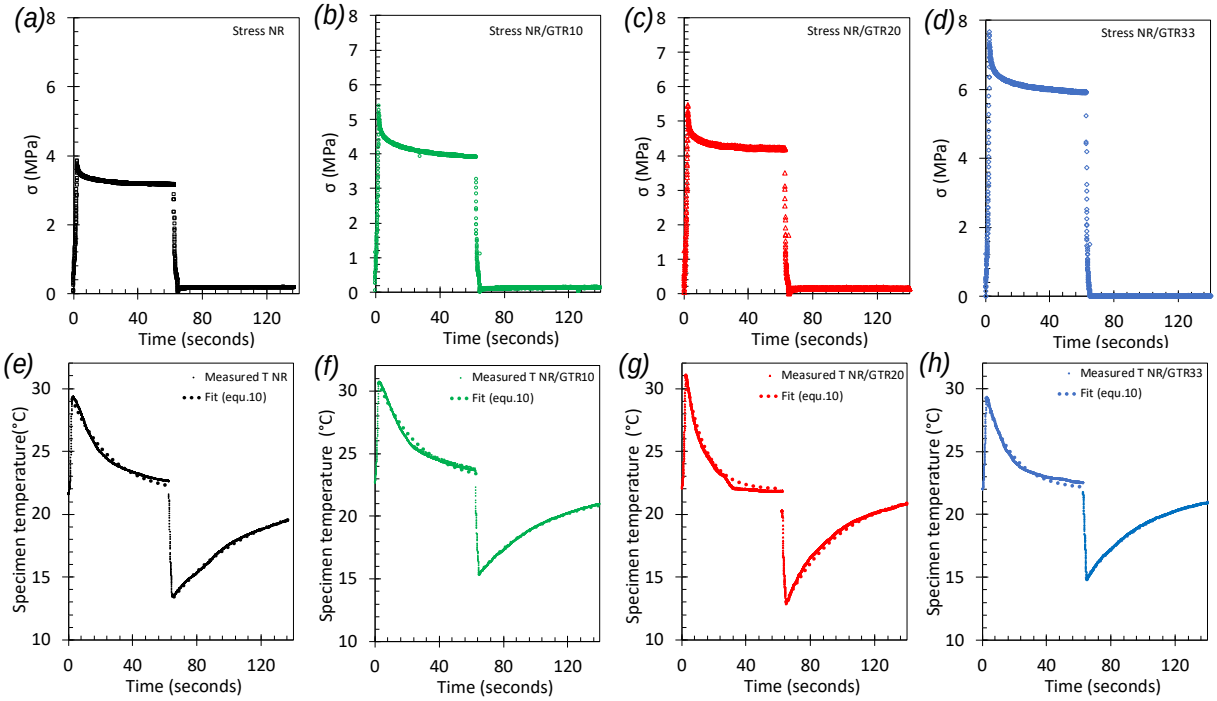

Figure 7. *(a, b, c, d)* stress versus during cycles (solid lines) performed at room temperature for the series of rubber from left to right: NR, NR/GTR10, NR/GTR20 and NR/GTR33. *(e, f, g, h)* corresponding temperature versus time (solid lines) at the specimen surface measured on the center of the specimen for the same materials. The detailed testing procedure for the cycles is given in the experimental section. The dotted lines correspond to the fitting of the return to equilibrium temperature during the phases of relaxation (right after the loading and unloading) using equations 4 and 5.

A maximum temperature rising of 0.4 °C is found for the natural rubber (NR) at a time around 700 msec (**Figure 8a**). Beyond such time, non-adiabatic conditions allow heat exchange within the environment that impedes to further track delayed crystallization using IR signal, Nonetheless, strain induced crystallization is known to still occur for longer relaxation times. Tosaka [50] showed that, after a rapid stretching of a rubber specimen, “fast” and “slow” crystallization processes may occur during the relaxation step, whose both are associated with characteristic times

of several hundred of milliseconds and several seconds respectively. Interestingly, the addition of waste rubber results in both a faster and lower maximum temperature rise during relaxation step, suggesting the SIC process to mainly occur during the loading while adding more GTR. This may be due to the strain amplification effect in presence of GTR particles that results in an increase characteristic time. Indeed, is has been shown that the SIC characteristic time is significantly shortened with applied strain [24].

In addition, it should be noted that strain induced crystallites formed during the loading phase of dynamic cycles may show some instabilities that accelerate their melting during unloading [53]. Such instabilities are expectedly due to delay in the crystallization during loading but are unlikely in our tests due to the application of the relation step in the deformed state. The application of a relaxation phase after loading is hence an important path to permit not only the completion of the crystalline phase but also the stabilization of formed strain induced crystals that will both benefit to the cooling performance. Finally, we verified that no trace of temperature changes is observed during the relaxation after unloading (**Figure 8b**) suggesting that the melting of stabilized crystallites occurs instantaneously during unloading (i.e., the time to unload the specimen is faster than the time of the melting process). As demonstrated by direct in situ X-Rays by Bruning et al. [51].the melting of strain induced crystals in natural rubber is complete within about 10 ms, a time much lower that unloading time in our experiments (around 2.4 seconds). This is thought to be beneficial for an efficient cooling, as all cumulated heat sink should happen within fast unloading step (see section 3.3).

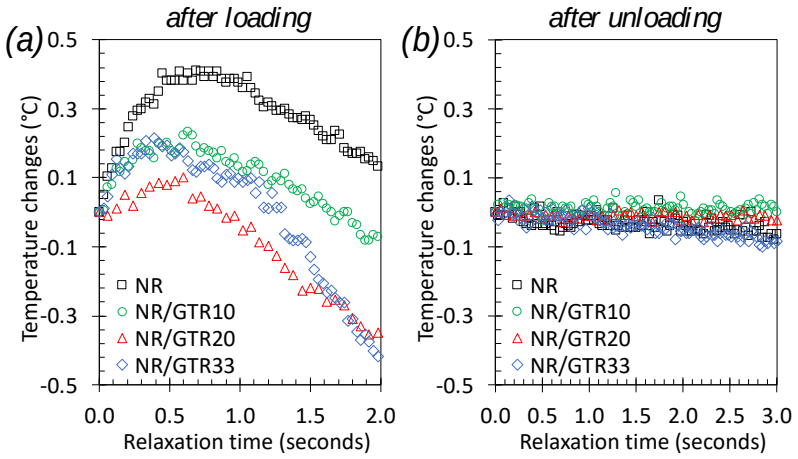

Figure 8. Temperature changes at the specimen center at the first times (up to 2 seconds) of the relaxation steps right after the loading (a) and unloading (b) for the four rubber blends tested.

3.3. Heat sources/ sink and elastocaloric performance in NR and NR/GTR blends

The calculation of heat source and sink is of prime importance to fully describe the eC phenomena in NR and NR/GTR and discriminate the diverse contribution of thermoelasticity, strain induced crystallization, melting, viscoelasticity and damage involved in the materials heating and cooling performances. Thermoelasticity and crystallization/melting are elastic reversible processes, while damage and viscoelasticity are inelastic processes. To estimate heat sources/sink, only the temperature at the specimen surface in the central part of the tensile bars is considered where the temperature field is spatially homogeneous (**Figure 1**). Hence, the heat source distribution is seen uniform within the considered area of interest. A linearization of heat losses in the heat equation results in the following expression of the heat source [54,55]:

$$S = \rho C \left(\dot{\theta} + \frac{\theta}{\tau(\lambda)} \right) \quad (9)$$

S is the heat source expressed in $MW.m^{-3}$, ρ is the bulk density ($g.cm^{-3}$) of the tested material, C its heat capacity ($J.g^{-1}K^{-1}$), $\theta=T-T_0$, the temperature variation above (positive) or below (negative) the equilibrium room temperature, T_0. $\dot{\theta}$ is the rate of heating ($K.s^{-1}$). The time constant τ (s)

characteristic of the heat exchange (during heating or cooling) along the specimen thickness was calculated using the following equation:

$$\theta = (T_{t=0} - T_0)e^{-}\frac{t}{\tau(\lambda)} \tag{10}$$

With $T_{t=0}$ the temperature at the beginning of the relaxation steps after the specimen has been heated (during loading) or cooled (during unloading). The constant time was calculated by using the fitting low in equation 10 to describe the time dependence of the return to equilibrium room temperature during the relaxation steps (see dotted lines in **Figures 7e-h**). This allowed us to determine the time constant for each material (**Figure 9a**) in the deformed state (500%) and in the relaxed state (zero force corresponding to deformations of approximately 80-90 %). One can note that such law is not universally used to quantify the return to room temperature of heated materials and is expected to depend on the heating conditions (self-heating or external heating), on the nature of the material and on the temperature measurement tool. The time dependence of the return to equilibrium of a polymer after external heat excitation have been found to follow logarithmic law [56] or inverse square root law [57]. We rather used a law that successfully fitted the return to equilibrium temperature of other elastomeric systems such as SBR [58,55] or NR [59]. The dependence of such time constant on the applied deformation was then evaluated assuming that this time will decrease similarly with the thickness reduction upon longitudinal deformation, $e = e_0/\sqrt{\lambda_1}$:

$$\tau(\lambda) = \frac{\tau(\lambda = 1)}{\sqrt{\lambda}} \tag{11}$$

The thickness reduction, and by inference the time constant reduction, is estimated here assuming the volume conservation of the material. The materials may however undergo volume changes due to both temperature dilatation crystallization/melting. Nonetheless, these are assumed negligible

as compared to thickness reduction due to stretching. For instance, the crystallization/melting of 10 vol.% of the rubber chains that can be expected in our materials results in a volume contraction/dilatation of only 2%. This means a thickness reduction of around 0.7% while a stretching up to λ=6 gives a thickness contraction of 40%. Moreover, the presence of crystal phase may modify the thermal properties of the studied materials (e.g., well-ordered and packed crystals favour heat conduction as compared to amorphous chains in the random coiled state), but the expected low amount of crystalline fraction generated (around 10-20 vol.%) is assumed to provide no drastic changes on the thermal properties.

The deformation dependence of the time constant (equation 11) is plotted for the NR and NR/GTR blends and found to satisfactorily follow the time constant estimations for both the relaxed state (80-90% deformation) and deformed state (500% deformation), meaning that the time decrease with strain is satisfactorily explained by equation 11 using the approximation of volume conservation. Interestingly, the time constant is found to decrease while adding waste rubber (**Figure 9b**), which is consistent with results found on than natural/wastes rubber blends used as a barocaloric material [32]. Due to concomitant increased density and decreased specific heat capacity by adding GTR particles, the resulting heat capacity if found to weekly dependent on the presence of GTR (**Table 1**). The acceleration of heat exchange is rather due to the increased thermal conductivity (**Table 1**) of the material in presence of GTR due to their content in carbon black particles [60]. It can be seen as a beneficial property for potential cooling devices by favouring the cooling transfer from the unloaded material to an external circulating fluid.

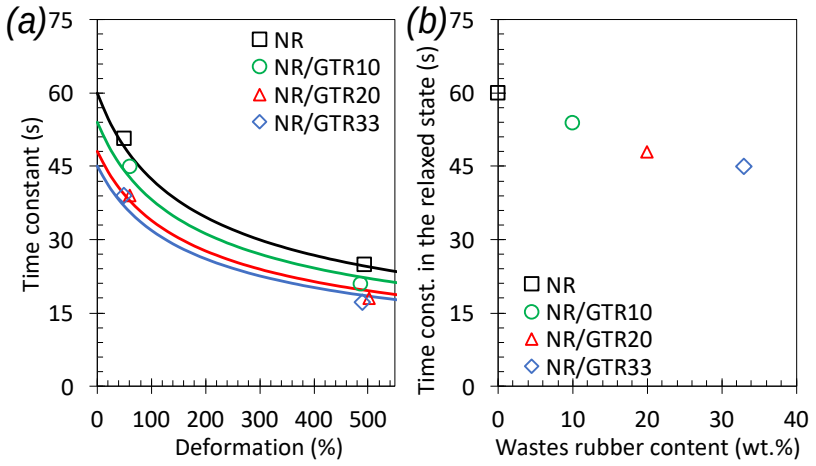

Figure 9. Time constant of return to equilibrium temperature estimated during the relaxation steps (right after loading in the deformed state at around 500% and right after unloading at zero force and a deformation below 100%). The experimental constant times were estimated using equations 10 and the fitting of deformation dependence using equation 11. A deformation, ε, from 0 to 500% correspond to a stretching ratio, λ, from 1 to 6.

The heat source/sink during loading/unloading obtained from equation 9 is presented for the NR and NR/GTR blends (**Figure 10**) as a function of the experimental time for the loading, relaxation after loading and unloading phases. A change in slope can be clearly seen during the loading phase, especially in the neat NR (**Figure 10a**) that corresponds to a transition from a dominant thermoelastic effects at lowest times to a dominant strain induced crystallization at the largest ones. We have seen that the adiabatic Gaussian approximation fits the stress-strain curve in fast loading conditions (**Figure 2**) and the resulting thermoelastic effects fit the temperature rise (**Figure 4**) at deformation up to 300%. The deformation energy (in $MJ.m^{-3}$) required to stretch the rubber specimen up to moderate deformations (below SIC onset), characteristic of thermoelastic effects, is written by integrating the gaussian stress over strain, and written as follows:

$$E_{th-e} = Q_{th-e} = \int_{t(\lambda=1)}^{t(\lambda_f)} \sigma_{g,4}\, d\lambda = \rho C \theta_{th-e} \qquad (12)$$

We assume here that the deformation energy associated with thermoelastic effects E_{th-e} is fully converted into heat, vi the heat exchange term Q_{th-e}. $\sigma_{g,4}$ is expressed in equation 5. Hence, assuming the thermoelastic process to be reversible, strain dependent but not time dependent (assumed to occur instantaneously within the loading or unloading), the heat source ($MW.m^{-3}$) resulting from thermoelastic effects can be written:

$$S_{th-e} \approx \frac{dE_{th-e}}{dt} = \rho C \dot{\theta}_{th-e} \tag{13}$$

With $\dot{\theta}_{th-e}$ is the derivation over time of the temperature changes due to thermoelastic effects defined in equation 7. The heat source S_{th-e} (equation 13, dotted lines in **Figure 10**) is found to well describe the total heat source *S* (equation 9, data points in **Figure 10**) at the first stage of loading. Above a certain time (around 1 second), the total heat source diverges that is due to strain induced crystallization. During the relaxation, heat source decreases down to zero. During unloading, the initial values of the heat sink are ascribed to the thermoelastic effects. Like for the loading, it then deviates, and heat sink is mostly ascribed to the melting of strain induced crystals.

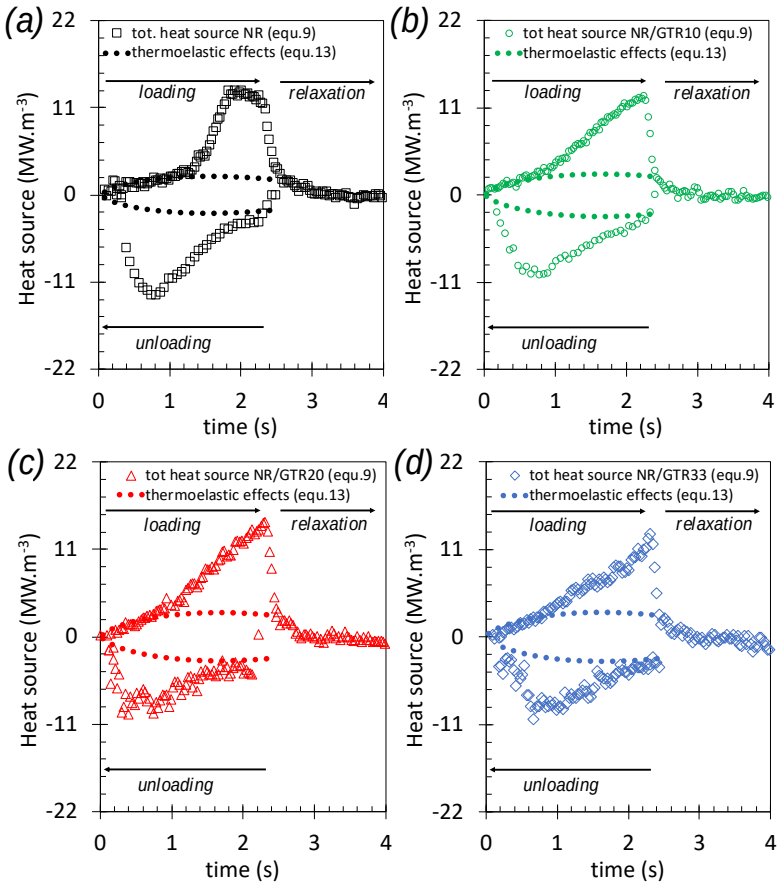

Figure 10. Total heat source calculated from the temperature on specimen surface and from equation 9 (data points) for the NR (a), NR/GTR10 (b), NR/GTR20 (c) and NR/GTR33 (d). The heat source estimated to account for thermoelastic effect within the gaussian approximation (equations 7-8) are given in dotted lines and the arrows indicate the strain at which a deviation between experimental curves and the gaussian approximation is observed.

The positive heat exchange Q^+ is calculated by integrating the heat source over time during both the loading and relaxation phase (we account here for the delayed crystallization that also contributes to the total heat source) and written:

$$Q^+ = \int_{t(\lambda=1)}^{t(\lambda_f)} S\,dt = Q_\chi + Q_{th-e} = \int_{t(\lambda=1)}^{t(\lambda_f)} S_\chi\,dt + \rho C\theta_{th-e} \tag{14}$$

With $Q_\chi$and $S_\chi$the heat change and heat source respectively ascribed to crystallization. Similarly, a negative heat exchange Q^- can be expressed accounting for thermoelastic effects and strain induced crystals melting during unloading:

$$Q^- = Q_m - Q_{th-e} \tag{15}$$

Heat exchange is represented in **Figure 11**. In order to visualize the reversibility of the heat source/sink due to crystallization/ melting, we represented $Q^+$for loading but $Q^+(\lambda_f) - Q^-$for unloading. $Q^+(\lambda_f) - Q^-$ is found to decrease down to zero at the end of unloading, confirming the reversibility of the heat sources, suggesting the absence of signature of irreversible thermal dissipation. The latter are generally induced by viscoelasticity and/or damage, as observed in conventional industrial carbon black filled Ethylene Propylene Diene Monomers (EPDM) [61,62] containing more significant amounts of CB (that can reach up to 80 phr against a maximum of 18 phr in our materials). In addition, industrial carbon black filled styrene butadiene rubber (SBR) with amounts of 30 phr show negligible cavitation [63] and weak Mullins hysteresis [64]. The crystallization and melting are found to be the first contribution to heat exchange and thermoelastic effects the second one. This is consistent with the literature for neat NR [65,66]. For the NR/GTR blends, this general trend also applies, while the contribution of thermoelastic effect is found to be more predominant when increasing the GTR content, likely due to the dependence of θ_{th-e} on the strain amplification factor (see equation 7). Finally, a maximum heat exchange is measured for the NR/GTR20 blend due to high contribution of thermoelastic effects and an optimum crystallization ability.

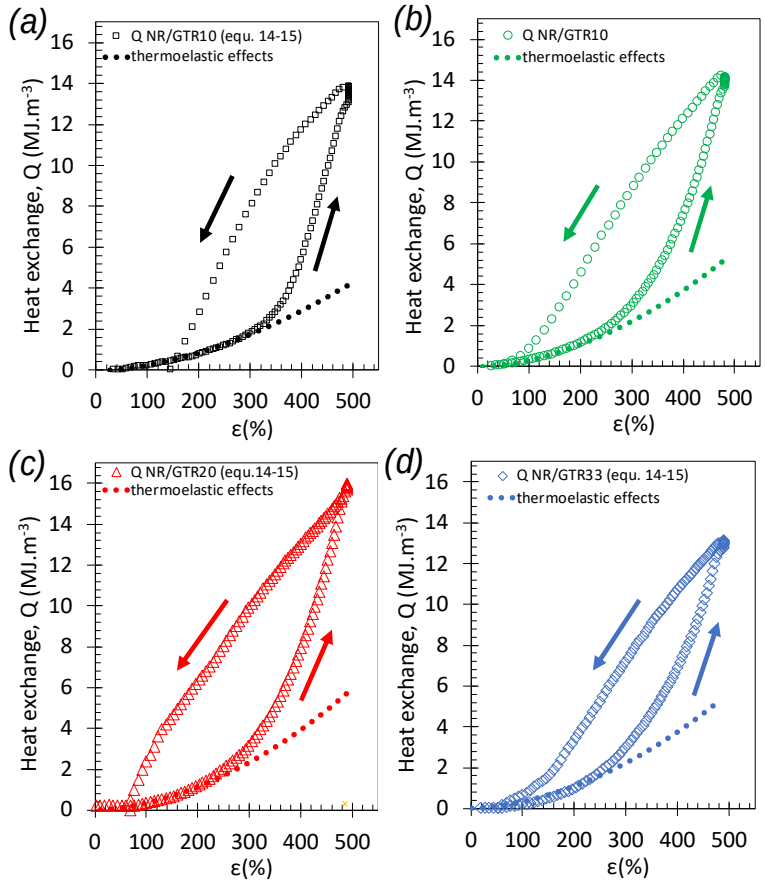

Figure 11. Heat exchange (MJ.m^{-3}) estimated for all blends (NR (a), NR/GTR10 (b), NR/GTR20 (c) and NR/GTR33 (d) from the integration over time of the total heat source (left hand of equation 13, and the heat exchange due to thermoelastic effects is estimated from the integration over time of the heat source associated with thermoelastic effects (equation 12) that simply writes as $\rho C\theta_{th-e}$ as shown in equation 13. A deformation, ε, from 0 to 500% correspond to a stretching ratio, λ, from 1 to 6.

The estimate of heat exchanges during loading and unloading as well as the identification of the thermoelastic contribution allow us to quantify the volume fraction of strain induced crystalline phase during loading, relaxation and unloading. It is usually assumed that the crystalline fraction is directly proportional to the temperature changes during rapid loading [65]. The volume crystalline fraction is then approximated by:

$$\chi \approx \rho C \frac{\theta_\chi}{\Delta H_m} \tag{16}$$

With ΔH_m=61 MJ.m^{-3} the melting enthalpy of vulcanized NR [67] and $\theta_{\chi=}\theta - \theta_{th-e}$, the temperature changes ascribed to strain induced crystallization. Equation 16 however cannot apply if long relaxation phases are applied (which is our case) where return to equilibrium temperature occurs for times in the range of the thermal diffusion time constant (see **Figure 9**). Moreover, in our NR/GTR blends, the crystalline fraction must be corrected to the presence of carbon black particles, hence only considering the rubber fraction, φ_r (**Table 1**). Accounting for these above-mentioned aspects, the crystallinity can be written into a more general equation:

$$\chi = \frac{Q_\chi}{\Delta H_m \varphi_r} = \frac{\int_{t(\lambda=1)}^{t(\lambda_f)} S_\chi dt}{\Delta H_m \varphi_\chi} = \frac{\rho C}{\Delta H_m \varphi_\chi} \int_{t(\lambda=1)}^{t(\lambda_f)} \left(\dot{\theta_\chi} + \frac{\theta_\chi}{\tau(\lambda)} \right) dt \quad (17)$$

Same formula is used to quantify the crystalline fraction during melting by substituting Q_χ by $Q_\chi(\lambda_f) - Q_m$. Equation 17 applied to crystallization process (loading and relaxation) and melting (unloading) is used to re-build the crystalline volume fraction (**Figure 12**). Crystallization is found to start at around 300% and strain at SIC onset seems to slightly decrease by adding GTR. The final crystalline fraction measured at the end of the loading stage is found to reach values around 12-17 vol.%. An optimum crystallinity of more than 17 vol.% is calculated for the NR/GTR20 blend, consistent with previously described optimum heat exchange due to *(i)* high thermoelastic effects in turn ascribed to strain amplification and *(ii)* an optimum crystallization process. A dedicated study of crystalline parameters (crystallites volume, crystallite number, crystallite orientation) by in situ X-Rays suggested this optimum to be due to a maximum number of SIC crystals measured in the NR/GTR20 [31].

One may note that, consistent with observed delayed temperature rise (**Figure 8a**), remaining crystallization occurs during the relaxation step to complete the crystalline fraction up to a maximum of 2 vol.% for neat NR. The delay effect is however less pronounced while increasing

the GTR content (see discussion about **Figure 8** in section 3.2). The crystallinity decreases down to zero during unloading, consistent with the previously discussed reversibility of the crystallization/melting processes. Finally, the deformation at complete melting estimated as the return to zero vol% of the crystalline fraction, occurs between 50 and 150% and found to decrease while increasing the GTR content. This can be ascribed, like for strain at SIC onset, to a strain amplification effect, that results in a higher thermal stability of the strain induced crystals through the lower local chains entropy (higher extension). This is however a first approximation, and the crystallites size (not estimated here), may also play a role in the thermal stability of the strain induced crystalline phase.

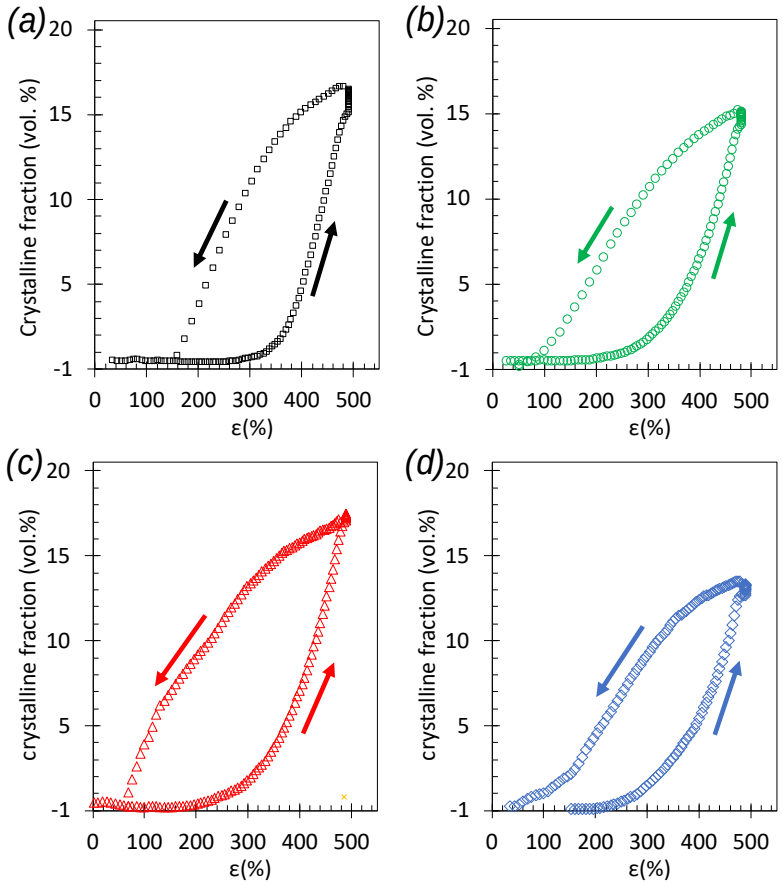

Figure 12. Crystalline fraction (vol.%) estimated for all blends (NR (a), NR/GTR10 (b), NR/GTR20 (c) and NR/GTR33 (d) from equation 16. A deformation, ε, from 0 to 500% correspond to a stretching ratio, λ, from 1 to 6.

From the knowledge of heat exchanges and the deformation energy, the heating/cooling performance in the NR and NR/GTR blends may be estimated. To this aim, the mechanical energy E_m (area under the tensile curve) is first estimated as follows:

$$E_m(\lambda) = \int_{t(\lambda=1)}^{t(\lambda_f)} \sigma \, d\lambda \tag{18}$$

The mechanical energy is shown in **Figure 13**. For sake of clarity, mechanical energy associated with thermoelastic effects are also plotted during the loading phase. From equation 12, the latter simply writes $E_{th-e} = \rho C \theta_{th-e}$. From **Figure 13**, several quantities can be discussed: mechanical dissipation and maximum deformation energy. The dissipated energy is obtained by direct lecture of the final energy value (measured at the end of unloading). One may note that, as thermoelastic effects are assumed reversible, they do not intervene in the dissipated energy. The latter is thus entirely ascribed to crystallization/melting processes. As crystallization and melting are not symmetrical (they do not occur at same strain due to "superstraining" effect) they induce such mechanical dissipation. The maximum applied mechanical energy, $E_{m(\lambda_f)}$, which is the mechanical energy measured at the end of the loading phase, is found to increase in presence of GTR, that is due to the reinforcing effects of the waste particles as they contain carbon black aggregates.

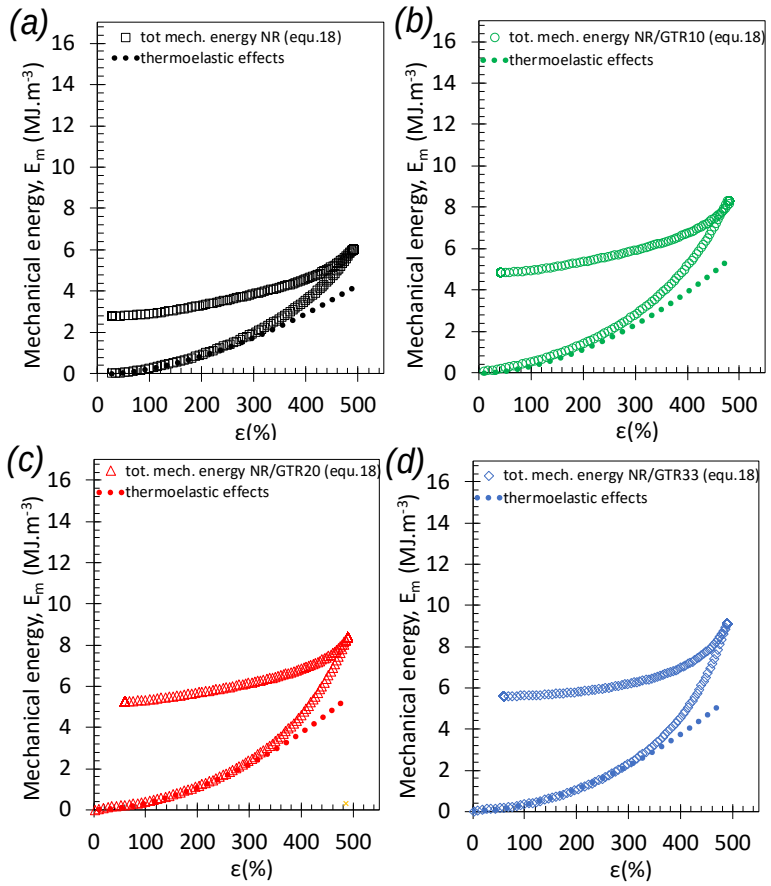

Figure 13. Mechanical energy (MJ.m^{-3}) estimated for all blends (NR (a), NR/GTR10 (b), NR/GTR20 (c) and NR/GTR33 (d) from the integration over stretching ratio of the stress-strain curves (left hand of equation 13, and the heat exchange due to thermoelastic effects is estimated from the integration over time of the heat source associated with thermoelastic effects (equation 12) that simply writes as $\rho C\theta_{th-e}$ as shown in equation 18. A deformation, ε, from 0 to 500% correspond to a stretching ratio, λ, from 1 to 6.

An estimation of the materials coefficient of performance, COP_{mat}, can be obtained according to the following equation:

$$COP_{mat} = \frac{Q^+ - Q^-}{E_{m(\lambda_f)}} \tag{19}$$

With $Q^+ - Q^-$ the amplitude of the heat exchanged during heating and cooling. One may note that such COP_{mat} value is only qualitative, and essentially used to compare our different materials. One

may refer to the study of Guyomar et al. for a proper estimate of the COP_{mat} value in natural rubber deduced from experiments performed at different temperatures [22]. Accounting for both crystallization/melting and thermoelastic contributions (see equations 14 and 15), COP_{mat} then writes:

$$COP_{mat} = \frac{Q_\chi - Q_m + 2\rho C\theta_{th-e}}{E_{m(\lambda_f)}} \tag{20}$$

A simplified expression, assuming fully adiabatic conditions (in case the thermal diffusion time is assumed much longer as compared to experimental time) results in a quite good assumption of the COP_{mat}:

$$COP_{mat} \approx \frac{\rho C\,(T_{max} - T_{min})}{E_{m(\lambda_f)}} \tag{21}$$

With T_{max} and T_{min}, the maximum and minimum temperatures respectively obtained after loading/ relaxation and unloading respectively. The maximum deformation energy, $E_{m(\lambda_f)}$, the positive heat exchange, Q^+, and the materials coefficient of performance, COP_{mat}, are shown (**Figure 14**). As commented above, the maximum deformation energy, is regularly increased while adding GTR particles. However, the heat exchange shows an optimum for the NR/GTR blends due to the cumulative effect of *(i)* a high thermoelastic effect due to strain amplification and *(ii)* a high crystalline fraction due to nucleating effect of the GTR particles. The NR/GTR33 shows the highest heat exchange due to thermoelastic effects but a lower ability to crystallize as compared to NR/GTR20 that likely results from a lower crystallization ability likely due to confinement effects in the NR matrix surrounded by a too low inter-particles distance. Thanks to its lowest deformation energy, the neat NR shows the best COP_{mat} value that is found around 4.4. Among the NR/GTR blends, the NR/GTR20 shows the best COP_{mat} value found equal to 3.8. The decent COP_{mat} value in the natural/wastes rubber blends as compared to the one in neat natural rubber, and the huge

temperature span during cyclic loading – found in the range of values for conventional elastocaloric systems, such as films of polycrystals [68] – make vulcanized natural/wastes rubber blends promising eco-friendly elastocaloric materials for cooling/ heating applications. One may note however that the effect of cyclic accumulation will need to be further studied, to investigate on suitable loading conditions for real heating/cooling systems. Fatigue behaviour in eC natural rubber had been studied and shows limitation as the specimen breaks after 800 cycles. However such limitation can be overcome by reducing the strain amplitude in a range of interest (e.g., from 300% to 600% deformation) resulting in an increase of fatigue life up to 3000 cycles [69].

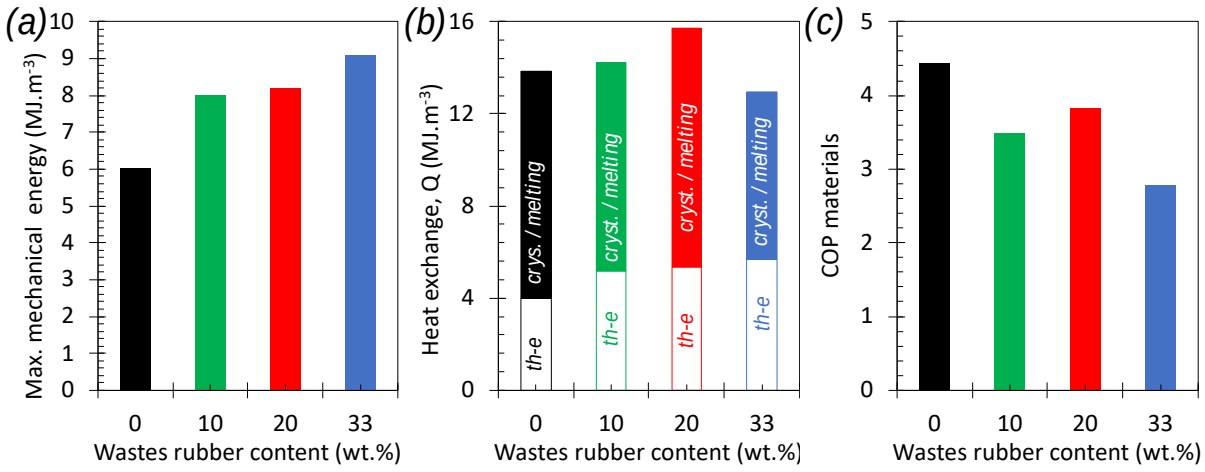

Figure 14. *(a)* Dissipated mechanical energy obtained from the area under the stress-strain curves (see **Figure 11**), *(b)* heat exchange measured at the end of the crystallization process (after loading and relaxation), or at the end of the melting during unloading. The contribution of the thermoelastic effect and crystallization/melting are reported. *(c)* the coefficient of performance COP_{mat} of the different blends NR, NR/GTR10, NR/GTR20 and NR/GTR33 obtained from equation 19.

4. Conclusion

The elastocaloric (eC) effect in vulcanized natural rubber (NR) and natural rubber / waste rubber blends (NR/GTR) was investigated by infrared thermography (IR) technique. This was combined with a thermodynamic frame allowing to quantify the mechanisms at the origin of heat exchanges

in these materials: *(i)* thermoelastic effects and *(ii)* strain induced crystallization/melting. We successfully modelled the stress strain curves, temperature rise, heat sources and heat exchanges by considering thermoelastic effects within the gaussian approximation up to deformation around 300%. Deviations of experimental data from this model was ascribed to the occurrence of strain induced crystals during loading and melting during unloading. From our approach, it resulted that both the thermoelastic effects and crystallization abilities progressively increased while increasing the quantity of waste particles (GTR) up to a content of 20 wt.%. This was explained by a strain amplification effect owing the presence of non-deformable carbon black aggregates in the waste particles. Given the large temperature span that remains in the range of the ones in conventional elastocaloric systems using rare earth elements, such as films of polycrystals, the prepared natural/wastes rubber blends can be proposed as candidates to contribute concomitantly to wastes recycling and to the development of novel sustainable energy technologies.

The presence of waste (GTR) particles raises the question on the temperature field heterogeneities at the scale of the waste particles as well as the efficiency of heat transfer between the natural rubber matrix and the waste particles. Further study is in progress to use an adapted IR camera configuration for the observation of the temperature field at the scale of the waste micro-particles. This would allow to identify the temperature cartographies able to give insight on local eC properties at the interface between the NR matrix and waste particle. Finally, for the design of a proper cooling device, in addition to the fatigue life optimization, the heat transfer parameters to the environment are to be carefully taken into account and the circulating fluid well chosen (adequate thermally conductive liquid).

5. Acknowledgements

The research leading to these results has received funding from the European Union's Horizon 2020 research and innovation programme under the Marie Skłodowska-Curie grant agreement No 712949 (TECNIOspring PLUS) and from the Agency for Business Competitiveness of the Government of Catalonia. Eduard Vives acknowledges Ministerio de Ciencia y Innovación (Spain) for financial support (project PID2020-113549RB-I00).

6. References

[1] B. Grocholski, « Cooling in a warming world », *Science*, vol. 370, nº 6518, p. 776-777, 2020, doi: 10.1126/science.abf1931.

[2] V. K. Pecharsky and K. A. Gschneidner Jr, « Magnetocaloric effect and magnetic refrigeration », *J. Magn. Magn. Mater.*, vol. 200, nº 1, p. 44-56, 1999, doi: 10.1016/S0304-8853(99)00397-2.

[3] K. Yang, C.-S. Yang, X.-X. Dong, Y.-H. Tan, Y.-Z. Tang, and W.-J. Wei, « Two Rare-Earth Molecular Ferroelectrics with High Curie Temperatures, Large Spontaneous Polarization, Switchable Second Harmonic Generation Effects, and Strong Photoluminescence », *Chem. Weinh. Bergstr. Ger.*, vol. 26, nº 26, p. 5887-5892, 2020, doi: 10.1002/chem.202000188.

[4] F. Greibich, R. Schwödiauer, G. Mao, D. Wirthl, M. Drack, R. Baumgartner, A. Kogler, J. Stadlbauer, S. Bauer, N. Arnold and M. Kaltenbrunner, « Elastocaloric heat pump with specific cooling power of 20.9 W g–1 exploiting snap-through instability and strain-induced crystallization », *Nat. Energy*, vol. 6, nº 3, p. 260-267, 2021, doi: 10.1038/s41560-020-00770-w.

[5] J. Gough, « A description of a property of Caoutchouc, or Indian rubber », *Mem. Lit. Philos. Soc. Manch.*, vol. 1, p. 288-295, 1805.

[6] J. P. Joule, « V. On some thermo-dynamic properties of solids », *Philos. Trans. R. Soc. Lond.*, vol. 149, p. 91-131, 1859, doi: 10.1098/rstl.1859.0005.

[7] S. L. Dart, R. L. Anthony, and E. Guth, « Rise of Temperature on Fast Stretching of Synthetics and Natural Rubbers », 2002. https://pubs.acs.org/doi/pdf/10.1021/ie50395a020

[8] P. J. Flory, « Thermodynamics of Crystallization in High Polymers. I. Crystallization Induced by Stretching », *J. Chem. Phys.*, vol. 15, nº 6, p. 397-408, 1947, doi: 10.1063/1.1746537.

[9] S. Trabelsi, P.-A. Albouy, and J. Rault, « Stress-Induced Crystallization Properties of Natural and Synthetic CIS-Polyisoprene », *Rubber Chem. Technol.*, vol. 77, nº 2, p. 303-316, 2004, doi: 10.5254/1.3547825.

[10] P.-Y. Le Gac, P.-A. Albouy, and D. Petermann, « Strain-induced crystallization in an unfilled polychloroprene rubber: Kinetics and mechanical cycling », *Polymer*, vol. 142, p. 209-217, 2018, doi: 10.1016/j.polymer.2018.03.034.

[11] F. Yeh, B. S. Hsiao, B. B. Sauer, S. Michel, and H. W. Siesler, « In-Situ Studies of Structure Development during Deformation of a Segmented Poly(urethane−urea) Elastomer », *Macromolecules*, vol. 36, nº 6, p. 1940-1954, 2003, doi: 10.1021/ma0214456.

[12] N. Candau, G Stoclet, J.F. Tahon, A. Demongeot, E. Yilgor, I. Yilgor, Y.Z. Menceloglu and O. Oguz, « Mechanical reinforcement and memory effect of strain-induced soft segment crystals in thermoplastic polyurethane-urea elastomers », *Polymer*, vol. 223, p. 123708, 2021, doi: 10.1016/j.polymer.2021.123708.

[13] N. Candau, L. Chazeau, J.-M. Chenal, C. Gauthier, and E. Munch, « A comparison of the abilities of natural rubber (NR) and synthetic polyisoprene cis-1,4 rubber (IR) to crystallize under strain at high strain rates », *Phys. Chem. Chem. Phys.*, vol. 18, nº 5, p. 3472-3481, 2016, doi: 10.1039/C5CP06383C.

[14] G. A. Holzapfel and J. C. Simo, « Entropy elasticity of isotropic rubber-like solids at finite strains », *Comput. Methods Appl. Mech. Eng.*, vol. 132, nº 1, p. 17-44, 1996, doi: 10.1016/0045-7825(96)01001-8.

[15] R. Laghmach, N. Candau, L. Chazeau, E. Munch, and T. Biben, « Phase field modelling of strain induced crystal growth in an elastic matrix », *J. Chem. Phys.*, vol. 142, nº 24, p. 244905, 2015, doi: 10.1063/1.4923226.

[16] J. Plagge and R. Hentschke, « Microphase Separation in Strain-Crystallizing Rubber », *Macromolecules*, 2021, doi: 10.1021/acs.macromol.1c00757.

[17] M. Tosaka, « Strain-Induced Crystallization of Crosslinked Natural Rubber As Revealed by X-ray Diffraction Using Synchrotron Radiation », *Polym. J.*, vol. 39, nº 12, Art. nº 12, 2007, doi: 10.1295/polymj.PJ2007059.

[18] B. Huneau, « STRAIN-INDUCED CRYSTALLIZATION OF NATURAL RUBBER: A REVIEW OF X-RAY DIFFRACTION INVESTIGATIONS », *Rubber Chem. Technol.*, vol. 84, nº 3, p. 425-452, 2011, doi: 10.5254/1.3601131.

[19] Z. Xie, G. Sebald, and D. Guyomar, « Elastocaloric effect dependence on pre-elongation in natural rubber », *Appl. Phys. Lett.*, vol. 107, nº 8, p. 081905, 2015, doi: 10.1063/1.4929395.

[20] D. Guyomar, Y. Li, G. Sebald, P.-J. Cottinet, B. Ducharne, and J.-F. Capsal, « Elastocaloric modeling of natural rubber », *Appl. Therm. Eng.*, vol. 57, nº 1, p. 33-38, 2013, doi: 10.1016/j.applthermaleng.2013.03.032.

[21] Z. Xie, G. Sebald, and D. Guyomar, « Comparison of elastocaloric effect of natural rubber with other caloric effects on different-scale cooling application cases », *Appl. Therm. Eng.*, vol. 111, p. 914-926, 2017, doi: 10.1016/j.applthermaleng.2016.09.164.

[22] Z. Xie, G. Sebald, and D. Guyomar, « Temperature dependence of the elastocaloric effect in natural rubber », *Phys. Lett. A*, vol. 381, nº 25, p. 2112-2116, 2017, doi: 10.1016/j.physleta.2017.02.014.

[23] G. Sebald, A. Komiya, J. Jay, G. Coativy, and L. Lebrun, « Regenerative cooling using elastocaloric rubber: Analytical model and experiments », *J. Appl. Phys.*, vol. 127, nº 9, p. 094903, 2020, doi: 10.1063/1.5132361.

[24] N. Candau, L. Chazeau, J.M. Chenal, C. Gauthier, J. Ferreira, E. Munch and C. Rochas, « Characteristic time of strain induced crystallization of crosslinked natural rubber », *Polymer*, vol. 53, nº 13, p. 2540-2543, 2012, doi: 10.1016/j.polymer.2012.04.027.

[25] European Commission, « A European Strategy for Plastics in a Circular Economy », 2018.

[26] M. Sienkiewicz, H. Janik, K. Borzędowska-Labuda, and J. Kucińska-Lipka, « Environmentally friendly polymer-rubber composites obtained from waste tyres: A review », *J. Clean. Prod.*, vol. 147, p. 560-571, 2017, doi: 10.1016/j.jclepro.2017.01.121.

[27] O. Oguz, N. Candau, M. K. Citak, F. N. Cetin, S. Avaz Seven, and Y. Z. Menceloglu, « A Sustainable Approach to Produce Stiff, Super-Tough, and Heat-Resistant Poly(lactic acid)-Based Green Materials », *ACS Sustain. Chem. Eng.*, vol. 7, nº 8, p. 7869-7877, 2019, doi: 10.1021/acssuschemeng.9b00319.

[28] N. Candau, O. Oguz, N. León Albiter, G. Förster, and M. L. Maspoch, « Poly (Lactic Acid)/Ground Tire Rubber Blends Using Peroxide Vulcanization », *Polymers*, vol. 13, nº 9, Art. nº 9, 2021, doi: 10.3390/polym13091496.

[29] S. Z. Salleh, M. Z. Ahmad, and H. Ismail, « Properties of Natural Rubber/Recycled Chloroprene Rubber Blend: Effects of Blend Ratio and Matrix », *Procedia Chem.*, vol. 19, p. 346-350, 2016, doi: 10.1016/j.proche.2016.03.022.

[30] G. Mathew, R. P. Singh, N. R. Nair, and S. Thomas, « Recycling of natural rubber latex waste and its interaction in epoxidised natural rubber », *Polymer*, vol. 42, nº 5, p. 2137-2165, 2001, doi: 10.1016/S0032-3861(00)00492-4.

[31] N. Candau, O. Oguz, C. E. Federico, G. Stoclet, J.-F. Tahon, and M. L. Maspoch, « Strain induced crystallization in vulcanized natural rubber containing ground tire rubber particles with reinforcement and nucleation abilities », *Polym. Test.*, vol. 101, p. 107313, 2021, doi: 10.1016/j.polymertesting.2021.107313.

[32] N. M. Bom, É.O. Usuda, M. Da Silva Gigliotti, D.J.M. De Aguiar, W. Imamura, L.S. Paixão and Carvalho, A.M.G., *2020* « Waste Tire Rubber-based Refrigerants for Solid-state Cooling Devices », *Chin. J Polym Sci2020 Vol 38 Pages 769-775*, vol. 38, nº 7, p. 769-775, 2020, doi: 10.1007/s10118-020-2385-y.

[33] J. Kruželák, R. Sýkora, and I. Hudec, « Peroxide vulcanization of natural rubber. Part I: effect of temperature and peroxide concentration », *J. Polym. Eng.*, vol. 34, nº 7, p. 617-624, 2014, doi: 10.1515/polyeng-2014-0034.

[34] L. A. Wood and N. Bekkedahl, « Specific heat of natural rubber and other elastomers aboved the glass transition temperature », *J. Polym. Sci. [B]*, vol. 5, nº 2, p. 169-175, 1967, doi: 10.1002/pol.1967.110050208.

[35] P. E. Khizhnyak, A. V. Chechetkin, and A. P. Glybin, « Thermal conductivity of carbon black », *J. Eng. Phys.*, vol. 37, nº 3, p. 1073-1075, 1979, doi: 10.1007/BF00861683.

[36] H. M. James and E. Guth, « Theory of the Elastic Properties of Rubber », *J. Chem. Phys.*, vol. 11, nº 10, p. 455-481, 1943, doi: 10.1063/1.1723785.

[37] M. Klüppel and J. Schramm, « A generalized tube model of rubber elasticity and stress softening of filler reinforced elastomer systems », *Macromol. Theory Simul.*, vol. 9, nº 9, p. 742-754, 2000, doi: 10.1002/1521-3919(20001201)9:9<742::AID-MATS742>3.0.CO;2-4.

[38] L. R. G. Treloar, *The Physics of Rubber Elasticity*. Oxford University Press, USA, 1975.

[39] A. Kloczkowski, M. A. Sharaf, and J. E. Mark, « Computer simulations on filled elastomeric materials », *Chem. Eng. Sci.*, vol. 49, nº 17, p. 2889-2897, 1994, doi: 10.1016/0009-2509(94)E0107-2.

[40] G. Kraus and J. T. Gruver, « Thermal expansion, free volume, and molecular mobility in a carbon black-filled elastomer », *J. Polym. Sci. Part -2 Polym. Phys.*, vol. 8, nº 4, p. 571-581, 1970, doi: 10.1002/pol.1970.160080408.

[41] E. Guth, « Theory of Filler Reinforcement », *Rubber Chem. Technol.*, vol. 18, nº 3, p. 596-604, 1945, doi: 10.5254/1.3546754.

[42] J. Diani, B. Fayolle, and P. Gilormini, « A review on the Mullins effect », *Eur. Polym. J.*, vol. 45, nº 3, p. 601-612, 2009, doi: 10.1016/j.eurpolymj.2008.11.017.

[43] N. Candau, O. Oguz, E. Peuvrel-Disdier, J.-L. Bouvard, C. Pradille, and N. Billon, « Strain and filler ratio transitions from chains network to filler network damage in EPDM during single and cyclic loadings », *Polymer*, vol. 197, p. 122435, 2020, doi: 10.1016/j.polymer.2020.122435.

[44] N. Candau, O. Oguz, E. Peuvrel-Disdier, J.-L. Bouvard, C. Pradille, and N. Billon, « Strain-induced network chains damage in carbon black filled EPDM », *Polymer*, vol. 175, p. 329-338, 2019, doi: 10.1016/j.polymer.2019.05.017.

[45] C. E. Federico, H.R. Padmanathan, O. Kotecký, R. Rommel, G. Rauchs, Y. Fleming and F. Addiego, « Resolving cavitation in silica-filled styrene-butadiene rubber composites upon

cyclic tensile testing », *Polym. Test.*, vol. 100, p. 107274, 2021, doi: 10.1016/j.polymertesting.2021.107274.

[46] Y. Ikeda, A. Kato, S. Kohjiya, and Y. Nakajima, *Rubber Science: A Modern Approach*. 2017, p. 220. doi: 10.1007/978-981-10-2938-7.

[47] J. R. Samaca Martinez, J.-B. Le Cam, X. Balandraud, E. Toussaint, and J. Caillard, « New elements concerning the Mullins effect: A thermomechanical analysis », *Eur. Polym. J.*, vol. 55, p. 98-107, 2014, doi: 10.1016/j.eurpolymj.2014.03.014.

[48] N. Candau, R. Laghmach, L. Chazeau, J.M. Chenal, C. Gauthier, T. Biben and E. Munch, « Strain-Induced Crystallization of Natural Rubber and Cross-Link Densities Heterogeneities », *Macromolecules*, vol. 47, nº 16, p. 5815-5824, 2014, doi: 10.1021/ma5006843.

[49] M. Tosaka, D. Kawakami, K. Senoo, S. Kohjiya, Y. Ikeda, S. Toki and B.S. Hsiao, « Crystallization and Stress Relaxation in Highly Stretched Samples of Natural Rubber and Its Synthetic Analogue », *Macromolecules*, vol. 39, nº 15, p. 5100-5105, 2006, doi: 10.1021/ma060407+.

[50] M. Tosaka, K. Senoo, K. Sato, M. Noda, and N. Ohta, « Detection of fast and slow crystallization processes in instantaneously-strained samples of cis-1,4-polyisoprene », *Polymer*, vol. 53, nº 3, p. 864-872, 2012, doi: 10.1016/j.polymer.2011.12.035.

[51] K. Brüning, K. Schneider, S. V. Roth, and G. Heinrich, « Kinetics of Strain-Induced Crystallization in Natural Rubber Studied by WAXD: Dynamic and Impact Tensile Experiments », *Macromolecules*, vol. 45, nº 19, p. 7914-7919, 2012, doi: 10.1021/ma3011476.

[52] N. Candau, R. Laghmach, L. Chazeau, J.M. Chenal, C. Gauthier and T. Biben, « Influence of strain rate and temperature on the onset of strain induced crystallization in natural rubber », *Eur. Polym. J.*, vol. 64, p. 244-252, 2015, doi: 10.1016/j.eurpolymj.2015.01.008.

[53] N. Candau, L. Chazeau, J.M. Chenal, C. Gauthier, J. Ferreira, E. Munch and D. Thiaudière, « Strain induced crystallization and melting of natural rubber during dynamic cycles », *Phys. Chem. Chem. Phys.*, vol. 17, nº 23, p. 15331-15338, 2015, doi: 10.1039/C5CP00384A.

[54] A. Benaarbia, A. Chrysochoos, and G. Robert, « Kinetics of stored and dissipated energies associated with cyclic loadings of dry polyamide 6.6 specimens », *Polym. Test.*, vol. 34, p. 155-167, 2014, doi: 10.1016/j.polymertesting.2014.01.009.

[55] J. R. Samaca Martinez, J.-B. Le Cam, X. Balandraud, E. Toussaint, and J. Caillard, « Filler effects on the thermomechanical response of stretched rubbers », *Polym. Test.*, vol. 32, nº 5, p. 835-841, 2013, doi: 10.1016/j.polymertesting.2013.04.003.

[56] W. Harizi, S. Chaki, G. Bourse, and M. Ourak, « Mechanical damage assessment of Polymer–Matrix Composites using active infrared thermography », *Compos. Part B Eng.*, vol. 66, p. 204-209, 2014, doi: 10.1016/j.compositesb.2014.05.017.

[57] Y. Y. Hung, Y.S. Chen, S.P. Ng, L. Liu, Y.H. Huang, B.L. Luk, R.W.L. Ip, C.M.L. Wu and P.S. Chung, « Review and comparison of shearography and active thermography for nondestructive evaluation », *Mater. Sci. Eng. R Rep.*, vol. 64, nº 5, p. 73-112, 2009, doi: 10.1016/j.mser.2008.11.001.

[58] J. R. Samaca Martinez, J.-B. Le Cam, X. Balandraud, E. Toussaint, and J. Caillard, « New elements concerning the Mullins effect: A thermomechanical analysis », *Eur. Polym. J.*, vol. 55, p. 98-107, 2014, doi: 10.1016/j.eurpolymj.2014.03.014.

[59] J. R. Samaca Martinez, J.-B. Le Cam, X. Balandraud, E. Toussaint, and J. Caillard, « Mechanisms of deformation in crystallizable natural rubber. Part 2: Quantitative calorimetric analysis », *Polymer*, vol. 54, nº 11, p. 2727-2736, 2013, doi: 10.1016/j.polymer.2013.03.012.

[60] Y. Agari and T. Uno, « Thermal conductivity of polymer filled with carbon materials: Effect of conductive particle chains on thermal conductivity », *J. Appl. Polym. Sci.*, vol. 30, nº 5, p. 2225-2235, 1985, doi: 10.1002/app.1985.070300534.

[61] N. Candau, O. Oguz, E. Peuvrel-Disdier, J.L. Bouvard, M.L. Maspoch, G. Corvec, C. Pradille, and N. Billon, « Heat source and voiding signatures of Mullins damage in filled EPDM », *Polym. Test.*, vol. 91, p. 106838, 2020, doi: 10.1016/j.polymertesting.2020.106838.

[62] N. Candau, O. Oguz, E. Peuvrel-Disdier, J.L. Bouvard, M.L. Maspoch, G. Corvec, C. Pradille, and N. Billon, « Effect of the Strain Rate on Damage in Filled EPDM during Single and Cyclic Loadings », *Polymers*, vol. 12, nº 12, Art. nº 12, 2020, doi: 10.3390/polym12123021.

[63] Y. Merckel, J. Diani, M. Brieu, and J. Caillard, « Effects of the amount of fillers and of the crosslink density on the mechanical behavior of carbon-black filled styrene butadiene rubbers », *J. Appl. Polym. Sci.*, vol. 129, nº 4, p. 2086-2091, 2013, doi: 10.1002/app.38925.

[64] Y. Merckel, J. Diani, M. Brieu, P. Gilormini, and J. Caillard, « CHARACTERIZATION OF THE MULLINS EFFECT OF CARBON-BLACK FILLED RUBBERS », *Rubber Chem. Technol.*, vol. 84, nº 3, p. 402-414, 2011, doi: 10.5254/1.3592294.

[65] J. C. Mitchell and D. J. Meier, « Rapid stress-induced crystallization in natural rubber », *J. Polym. Sci. Part -2 Polym. Phys.*, vol. 6, nº 10, p. 1689-1703, 1968, doi: 10.1002/pol.1968.160061001.

[66] J.-B. Le Cam, P.-A. Albouy, and S. Charlès, « Comparison between x-ray diffraction and quantitative surface calorimetry based on infrared thermography to evaluate strain-induced crystallinity in natural rubber », *Rev. Sci. Instrum.*, vol. 91, nº 4, p. 044902, 2020, doi: 10.1063/1.5141851.

[67] H. Kim and L. Mandelkern, « Multiple melting transitions in natural rubber », *J. Polym. Sci. Part -2 Polym. Phys.*, vol. 10, nº 6, p. 1125-1133, 1972, doi: 10.1002/pol.1972.160100614.

[68] M. Imran and X. Zhang, « Reduced dimensions elastocaloric materials: A route towards miniaturized refrigeration », *Mater. Des.*, vol. 206, p. 109784, 2021.

[69] G. Sebald, Z. Xie, and D. Guyomar, « Fatigue effect of elastocaloric properties in natural rubber », *Philos. Trans. R. Soc. Math. Phys. Eng. Sci.*, vol. 374, nº 2074, p. 20150302, 2016, doi: 10.1098/rsta.2015.0302.